Macromolecules

Article

pubs.acs.org/Macromolecules

Temperature-Variable FTIR and Solid-State ^{13}C NMR Investigations on Crystalline Structure and Molecular Dynamics of Polymorphic Poly(L-lactide) and Poly(L-lactide)/Poly(D-lactide) Stereocomplex

Pengju Pan,*[,†] Jinjun Yang,[‡,§] Guorong Shan,[†] Yongzhong Bao,[†] Zhixue Weng,[†] Amin Cao,[⊥] Koji Yazawa,[‡] and Yoshio Inoue[‡]

[†]State Key Laboratory of Chemical Engineering, Department of Chemical and Biological Engineering, Zhejiang University, 38 Zheda Road, Hangzhou 310027, China

[‡]Department of Biomolecular Engineering, Tokyo Institute of Technology, 4259-B-55 Nagatsuta, Midori-ku, Yokohama 226-8501, Japan

[§]School of Environmental Science and Safety Engineering, Tianjin University of Technology, Tianjin 300384, China

[⊥]Laboratory for Polymer Materials, Shanghai Institute of Organic Chemistry, Chinese Academy of Sciences, Shanghai 200032, China

Supporting Information

ABSTRACT: Crystalline structure and molecular dynamics in α and α' crystals of poly(L-lactide) (PLLA) and PLLA/poly(D-lactide) (PDLA) stereocomplex (sc) crystals have been investigated by the temperature-variable FTIR and solid-state ^{13}C CP-MAS NMR spectroscopy. The crystal forms of polylactide (PLA) have different band frequencies, correlation field splittings in FTIR spectra and different line shapes, and resonance splittings in solid-state NMR spectra, which become more distinct with cooling to the cryogenic conditions. The well-resolved splittings in NMR resonances of α crystals, attributable to the crystallographically inequivalent sites within crystal unit cell, are considered to be due to the dipolar interactions related to the carbonyl, methyl, and methine groups. The splittings in FTIR bands and NMR resonances are absent in α' crystals, indicating the disordered conformation and loose molecular lateral packing within their crystal lattices. The significant FTIR frequency shifts of ν(C═O), ν(CH$_3$), and ν(CH) modes during stereocomplex crystallization of PLLA/PDLA blend and the appearance of spectral splittings at cryogenic conditions suggest the coexistence of weak C−H···O═C hydrogen bonds and dipolar interactions between PLLA and PDLA chains in the sc crystals of PLA. Below the glass transition temperature (T_g), the spin−lattice relaxation times of PLA with different crystalline structures increase in the order of amorphous ≈ α' < α < sc.

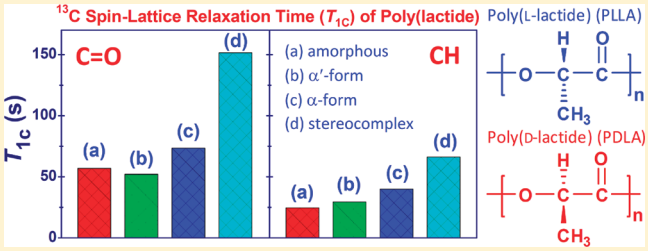

INTRODUCTION

Polylactide or poly(lactic acid) (PLA) has been considered as one of the most promising bio-based thermoplastics because its monomer, lactic acid, can be produced from renewable resources (e.g., starchy materials and sugars). The attributes of biodegradability, biocompatibility, good mechanical properties, and versatile fabrication processes make it a promising material for biomedical applications (e.g., implant materials, surgical suture, and controlled drug delivery systems) and commodity applications in substitution of the conventional oil-based thermoplastics.[1] Since lactic acid is a chiral molecule, the stereoregular PLA exists in two enantiomeric isomers, poly(L-lactide) (PLLA) and poly(D-lactide) (PDLA).

One of the most remarkable issues regarding the solid-state structure of PLA is its crystal polymorphism. The common stereoisomer of PLA, i.e., PLLA, can crystallize in α,[2−6] β,[7,8] and γ[9] polymorphs, depending on the crystallization conditions. The usual polymorph, α form, generally produced from the cold, melt, or solution crystallization, is characterized by an orthorhombic (or pseudo-orthorhombic) unit cell packed by two antiparallel left-handed helical chains in a distorted 10_3 conformation.[2−6] The β form, adopting a 3_1 helical conformation, can be attained via stretching its α counterpart at high temperature to a high drawing ratio.[7,8] Very recently, a metastable α' form has been proposed for the stereoregular PLA melt-crystallized at low crystallization temperature T_c (<100 °C) compared to the normal α crystals produced at high T_c (>120 °C).[10−15]

A wide range of physical properties such as thermal, mechanical, and electrical properties are influenced by the crystal modifications of polymorphic polymers.[16] In addition, crystalline structure is a key factor for the hydrolytic and enzymatic degradations of biodegradable polymers.[17,18] In the case of PLLA, Kanamoto and co-workers have reported that the

Received: August 21, 2011
Revised: December 2, 2011
Published: December 19, 2011

β-form PLLA had a higher tensile strength and modulus than its α counterpart.[19] Cocca et al. have reported that α-form PLLA possessed a higher Young's modulus and a better barrier to water vapor than its α′ counterpart.[20] Therefore, study on the relationships between crystal structure and crystallization condition is of fundamental importance because it allows for tuning the physical performances of polymeric materials by controlling their processing conditions. In the practical melt processing, stereoregular PLA is usually molded at 100−120 °C because of the relatively fast crystallization over this temperature region. The α′ and α mixed crystals are generally produced in this temperature range.[12−15] Therefore, study on the solid-state structure of α′ and α crystals of PLA would be important from the perspective of practical applications.

Previous studies have reported that the α′ and α crystals of PLA have different crystallization kinetics and thermal stability.[12−15,21] From the wide-angle X-ray diffraction (WAXD) and Fourier transform infrared (FTIR) spectroscopy analyses, it has been proposed that the α′ and α crystals have similar chain conformation and orthorhombic unit cell,[10,11] while the lateral dimension of α′ crystal lattice is slightly larger than that of its α counterpart.[12−14] On the basis of the infrared and Raman spectroscopic analyses, Hsu and co-workers[21] have recently found that the α′ crystals have conformational disorder and the disorder in chain packing and conformation results in the different crystalline forms. Because of the very similar WAXD patterns of α′ and α crystals, their structural difference is relatively difficult to elucidate, and many aspects still remain unclear. On the other hand, a notable structural feature of PLLA α crystals is the deviation of crystal system from the normal orthorhombic unit cell and the torsion of helix conformation.[2−6] The WAXD pattern of α-form PLLA displays some extra meridional reflections on the layer lines, indicating some extent of helix distortion from the pure 10_3 conformation.[2−4] The reason for helix distortion is still under debate. Hoogsteen et al. have suggested that the interchain interactions between methyl groups may force this distortion because a 10_3 helix with twisted grooves restricts the translation of neighboring chains with respect to each other by a kind of interlocking of methyl groups.[3] Puiggali et al.[5] as well as Sasaki and Asakura[6] have found the molecular distortion in the α crystals of PLLA, which is resulted by the asymmetric interchain interactions. More well-established experiments are required to elucidate the structural features of α′ and α crystals as well as the structural differences between them.

The PLLA/PDLA stereocomplex (sc) is another crystalline form of PLA. It is generally produced in the crystallization of 1:1 PLLA/PDLA blend from melt or solution.[22] Sc form is characterized by a triclinic unit cell packed by one PLLA and one PDLA chain, both adopting a 3_1 conformation.[22] A characteristic feature of sc form is its high melting point T_m, higher by ∼50 °C than those of the homocrystals. Compared to the homocrystals, sc crystals possess higher thermal stability, mechanical strength, tensile modulus, and hydrolytic and enzymatic degradation resistance.[23] The promising physical properties of sc-form PLA are due in part to the specific molecular packing and interchain interactions (e.g., van der Waals interactions[24] or interchain hydrogen bonds[25,26]) between the left- and right-handed helices of PLLA and PDLA chains. From this viewpoint, study on the crystal structure of sc crystals would shed light on the structure−property relationships of PLA materials.

High-resolution solid-state nuclear magnetic resonance (NMR) spectroscopy has revealed a high sensitivity to the microstructures of polymer chains in solid, and it is a powerful tool to study the molecular dynamics and relaxation.[27] With aid of this technique, the conformation, molecular packing, intrachain, and interchain interactions in the different crystal modifications of isotactic polypropylene (i-PP),[28−30] syndiotactic polypropylene (s-PP),[31,32] and isotactic poly(1-butene) (i-PB)[33] have been successfully investigated; some of this structural information cannot be attained from the diffraction techniques. Although several authors have reported the solid-state ^{13}C NMR spectra of α[34−36] and sc-form[37] PLAs, a systematic analysis and comparison of spectral features and molecular dynamics between the α′, α, and sc-form PLAs have been unexplored.

Experimental studies[38,39] and theoretical calculations[40] have indicated that the polymer crystals undergo a thermal anisotropic expansion or contraction with the temperature changes. This process can lead to the changes of crystal lattice spacing, conformational characteristics, and intrachain or interchain interactions, which in turn result in the alterations of macroscopic properties (e.g., mechanical properties[40]). Accordingly, FTIR[38,41−43] and NMR[30,33] studies with the temperature-variable techniques can provide new insights into the structural features of polymer crystals, particularly for the different crystal modifications of a given polymer. In this work, the solid-state structures of different crystalline forms (α′ and α crystals) of PLLA and sc crystals of PLLA/PDLA blend were investigated and analyzed using the temperature-variable FTIR and solid-state ^{13}C NMR techniques over a wide temperature range (140 to −140 °C). Molecular dynamics of these crystal forms were analyzed by the ^{13}C spin−lattice relaxation measurements. Based on these results, the structural features such as molecular packing, interaction, and mobility of different crystals of PLA were discussed.

EXPERIMENTAL SECTION

Materials. PLLAs with a low and high molecular weights, PLLA-L (M_n = 15.4 kg/mol, M_w/M_n = 1.38) and PLLA-H (M_n = 118 kg/mol, M_w/M_n = 1.49), were kindly supplied by Unitika Co. Ltd. (Kyoto, Japan). The L-isomer content in PLLA was ∼99.5%. PDLA (M_n = 23.0 kg/mol, M_w/M_n = 1.33) was synthesized via the ring-opening polymerization (ROP) of D-lactide (PURAC, The Netherlands). The samples were purified by precipitation into ethanol from the chloroform solution and then were dried under vacuum at 70 °C for 48 h.

Preparation of Various Crystal Forms of PLA. The α′- and α-form PLAs were prepared by the isothermal melt crystallization of PLLA-H at 80 and 140 °C for 6 h after melting at 200 °C for 2 min, respectively. To prepare the sc-form PLA, equivalent amounts of PLLA-L and PDLA were dissolved in chloroform (∼1 g/50 mL). The solution was cast on a Petri dish, and the solvent was allowed to evaporate under ambient conditions. It was then dried in a vacuum oven at 70 °C for 48 h. Sc-form PLA was prepared by isothermal melt crystallization of 1:1 PLLA-L/PDLA blend at 200 °C for 2 h under the protection of dry N_2 after melting at 240 °C for 2 min. Amorphous PLLA-H and 1:1 PLLA-L/PDLA blend samples were prepared by quenching from 200 and 240 °C to ∼25 °C, respectively. Unless otherwise specified, the sample "amorphous PLA" represents amorphous PLLA-H quenched from the melt.

Measurements. Differential Scanning Calorimeter. The measurements of differential scanning calorimeter (DSC) were performed on a Pyris Diamond DSC instrument (Perkin-Elmer Inc., Waltham, MA) equipped with an intracooler cooling accessory. The temperature and heat flow were calibrated by the indium standard at different heating rates. The preweighted sample (∼7 mg) was sealed in

an aluminum pan and then heated from 0 to 200 °C for amorphous, α′-form, and α-form PLAs or 250 °C for sc-form PLA at a heating rate of 10 °C/min to observe the melting behavior.

FTIR Spectroscopy. FTIR measurements were performed on a FTIR-6100 spectrometer (JASCO, Japan) equipped with an IMV-4000 multichannel infrared microscope (JASCO, Japan) and a MCT detector worked in the transmission mode. PLLA-H or 1:1 PLLA-L/PDLA blend sample was sandwiched by two BaF_2 windows and then melt-crystallized at the corresponding temperatures to prepare the α′-, α-, and sc-form PLAs or quenched to ∼25 °C from melt to prepare the amorphous sample, as above mentioned. The sample is thin enough to follow the Beer−Lambert law. The sample was cooled from 140 °C (for α and sc form), 80 °C (for α′ form), or 40 °C (for amorphous sample) to −140 (or −100) °C at a cooling rate of 5 °C/min in a LK-600 hot stage (Linkam Scientific Instrument Ltd., Surrey, UK) equipped with a L600A liquid N_2 cooling unit. FTIR spectra were recorded during the cooling process. The spectra were registered with 64 scans and a resolution of 2 cm^{-1}, and 4 data points were collected within each frequency interval of 2 cm^{-1}.

Solid-State NMR Spectroscopy. Solid-state ^{13}C NMR spectra were acquired on a JEOL JNM-ECA 500 MHz spectrometer operating at 500 MHz for ^1H and 125.8 MHz for ^{13}C using the cross-polarization (CP), magic-angle spinning (MAS), and high-power ^1H decoupling. CP-MAS spectra were measured with a 3.1 μs ^1H π/2 pulse, a 3 ms CP pulse with a 7% ramp on the ^1H channel and an rf field strength of 65 kHz, a MAS speed of ∼5 kHz, and a 5 s recycle delay. Two-pulse phase modulated (TPPM) ^1H decoupling with a 15° phase shift and a rf field strength of 80 kHz was applied during acquisition. ^{13}C chemical shift was referenced externally to the methyl carbon resonance of hexamethylbenzene at 17.4 ppm. The ^{13}C spin−lattice relaxation times (T_{1C}s) were measured at ∼25 °C with a conventional CPT1 pulse sequence reported by Torchia.[44]

RESULTS AND DISCUSSION

DSC Melting Behavior. Figure 1 shows the DSC heating curves of α′-, α-, and sc-form PLAs. The DSC curve of amorphous PLA is included for comparison. The thermal parameters including crystallization temperature (T_c) used for the sample preparation, melting point (T_m), melting enthalpy (ΔH_m), and degree of crystallinity (X_c) of three crystal forms of PLA are summarized in Table 1. X_c was estimated by comparing the ΔH_m value with the value of an infinitely large crystal (ΔH_m^0), which was taken as 93 J/g[45] for the α′ and α homocrystals and 142 J/g[46] for the sc crystals. Sc crystals exhibit a melting point at 232 °C that is more than 50 °C higher than the homocrystals. The DSC curve of α′ crystals shows an exotherm (P_{ex}) prior to the dominant melting peak, corresponding to the α′-to-α crystalline phase transition.[12−15] Because of the α′-to-α transition upon heating, the melting point observed from the DSC curve of α′ crystals corresponds to the α crystals developed in phase transition. ΔH_m values of the prepared crystal forms of PLA increase in the order of α′ < α < sc, exhibiting the same tendency to melting point and thermal stability.

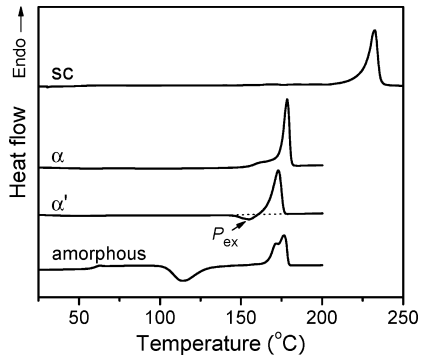

Figure 1. DSC heating curves of amorphous, α′-, α-, and sc-form PLAs recorded at a heating rate of 10 °C/min.

Table 1. Thermal Parameters of α′, α, and sc Crystals of PLA

crystal form	composition	T_c (°C)	T_m (°C)	ΔH_m (J/g)	X_c (%)
α′	PLLA	80	173	41	44
α	PLLA	140	179	62	67
sc	1:1 PLLA/PDLA	200	232	80	56

Temperature-Dependent FTIR Spectra. We first compared the FTIR spectra of amorphous, α′-, α-, and sc-form PLAs, as shown in Figure 2. As expected, the amorphous PLA and 1:1 PLLA/PDLA blend prepared by quenching exhibit the same FTIR spectra, since PLLA and PDLA are identical from a spectroscopic point of view. So, we used the quenched PLLA as a representative amorphous PLA sample to make a comparison to the crystalline ones. FTIR spectra are sensitive to the crystal forms of PLA (Figure 2), which will be discussed in combination with the temperature-dependent spectra in the following sections.

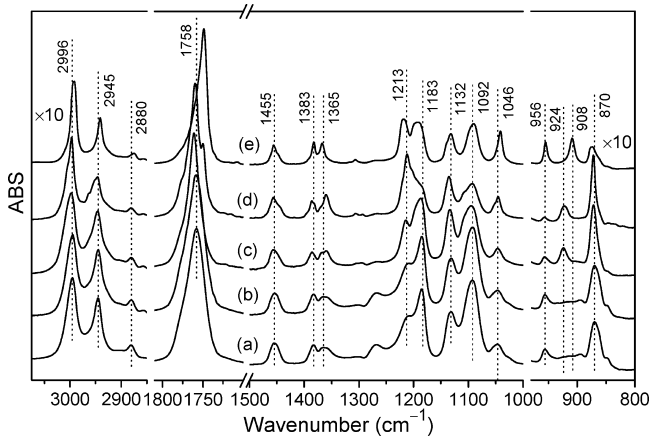

Figure 2. FTIR spectra of (a) amorphous PLLA, (b) amorphous 1:1 PLLA/PDLA blend, (c) α′-, (d) α-, and (e) sc-form PLAs collected at ∼25 °C. Spectral intensities in the wavenumber regions of 3075−2850 and 980−800 cm^{-1} were magnified by 10 times.

The crystalline structures of different PLA crystals were investigated by temperature-variable FTIR spectroscopy over the temperature range of 140 to −140 °C. The temperature-dependent FTIR spectra and their corresponding second derivatives for different crystals of PLA are shown in Figure 3 and Figures S1−S3. Assignments of FTIR bands for amorphous and crystalline PLAs are summarized in Table 2.[47] Considering the band frequency shift with temperature, the wavenumbers shown in Figure 3 and Table 2 were derived from the spectra collected at 20 °C. As seen in Figure 3 and Figure S1, aside from the spectral intensity and band frequency, the line shape of α′ crystals is nearly unaltered with cooling from 80 to −140 °C. This is similar to the amorphous PLA (data not shown). In contrast, the line shape of α crystals varies remarkably with temperature (Figure 3 and Figure S2). Its spectrum splits into quite a few new components with cooling to −140 °C, such as the components at 3006 cm^{-1} of $\nu_{as}(CH_3)$, 2964 cm^{-1} of $\nu_s(CH_3)$, 1777 and 1749 cm^{-1} of $\nu(C{=}O)$, 1468 and 1443

dx.doi.org/10.1021/ma201906a | Macromolecules 2012, 45, 189−197

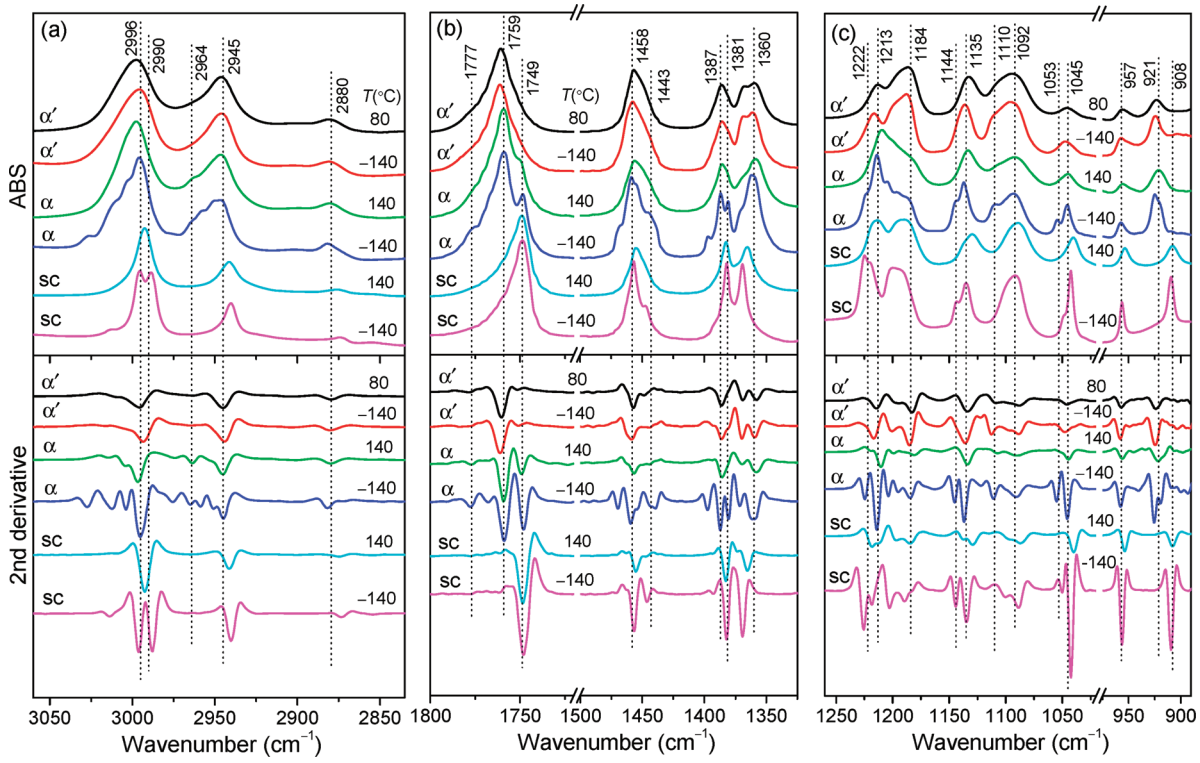

Figure 3. Temperature-dependent FTIR spectra and their second derivatives of α'-, α-, and sc-form PLAs. Intensities of FTIR spectra and their second derivatives in the wavenumber ranges of 1500−1325 and 975−890 cm^{-1} were magnified for clarity.

cm^{-1} of $\delta_{as}(CH_3)$, 1396 and 1381 cm^{-1} of $\delta_s(CH_3)$, 1222 cm^{-1} of $\nu_{as}(COC)$ + $r_{as}(CH_3)$, 1144 cm^{-1} of $r_{as}(CH_3)$, and 1053 cm^{-1} of $\nu(C-CH_3)$ (Table 2). These splitting bands can be identified distinctly from the second derivatives of original FTIR spectra at low temperature (e.g., below −40 °C), as shown in the lower panels of Figure 3 and Figure S2. Most of these splitting components cannot be observed at high temperature (e.g., above 80 °C). The pure crystalline band of α crystals at 924 cm^{-1}, which is absent in the spectrum of amorphous PLA (Figure 2) and associated with the combination of $r(CH_3)$ and $\nu(C-COO)$ modes of molecular chains with the 10_3 helix conformation in crystalline phase of PLA,[10,47] also splits into a doublet (924, 919 cm^{-1}) at low temperature.

A remarkable difference between the temperature-dependent FTIR spectra of α' and α crystals is the spectral splitting. So far, two interpretations, that is, the intrachain coupling and interchain coupling (i.e., correlation field splitting),[48,49] have been proposed to explain the vibrational splitting of $\nu(C{=}O)$ mode in the α-form PLLA. The former is sensitive to chain conformation and the distribution of conformers. The correlation field splitting, also called as factor group splitting or Davydov splitting, occurs due to the lateral interactions between the molecular chains contained in a crystal unit cell.[50] It has been reported that the unit cell dimension of polymer crystals along molecular axis (c-axis) is much less sensitive to temperature than is the transverse axes (a- or b-axis).[39,40] The chain conformation of crystalline PLA, which is sensitive to the length of c-axis and a key factor for intramolecular interactions, would not change markedly upon cooling. Furthermore, the temperature dependence of spectral splitting is a characteristic phenomenon of correlation field splitting.[50] Therefore, it is reasonable to conclude that the spectral splitting in α crystals is originated from the correlation field splitting, rather than the intrachain coupling. The correlation field splitting in α-form PLA is mainly resulted by the interchain dipolar interactions between the dipolar groups (carbonyl, methyl, and methine groups) of adjacent molecular chains packed within the crystal unit cells.[49]

The absence of correlation field splitting in α' crystals suggests the much weakened interchain interactions in its crystal lattice. This is due in part to the larger lattice dimension and interchain distance,[12−14] as evidenced by WAXD analysis. On the other hand, since the correlation field splitting usually takes place in an ordered structure with tightly packed molecular chains, the absence of spectral splitting may suggest the lateral disordered and loose molecular packing of the α' crystals. The molecular packing is considered to be a key factor influencing the polymorphism of PLA, analogous to the cases of i-PP[28,29] and aliphatic polyketones derived from ethene and carbon monoxide (ECO).[50] The α and β crystals of ECO possess the similar all-trans conformation, while due to the interchain dipolar interactions, the α crystals of ECO with tight molecular packing have more evident band splitting in Raman spectra than their β counterparts.[50]

Sc crystals of PLA exhibit different FTIR spectra from the homocrystals. First, one can clearly identify a new band at 908 cm^{-1} (Figures 2 and 3c), which is characteristic of the sc crystals with a 3_1 helical chain conformation.[47] This band has been observed for the β-form PLLA that adopts a similar 3_1 helical conformation.[8] Second, compared to the amorphous, α'-, and α-form PLAs, the band wavenumber of $\nu(C{=}O)$ mode in sc form is ~10 cm^{-1} lower and those of $\nu_{as}(CH_3)$, $\nu_s(CH_3)$, and $\nu(CH)$ modes are 4−6 cm^{-1} lower (Figure 3 and Table 2). The distinct low-frequency shifts of $\nu(C{=}O)$, $\nu(CH_3)$, and $\nu(CH)$ modes in the stereocomplex crystallization suggest the

dx.doi.org/10.1021/ma201906a | Macromolecules 2012, 45, 189−197

Table 2. Assignments of FTIR Bands for Amorphous, α′-, α-, and sc-Form PLAs

vibration modes	amorphous	α′	α	sc
$\nu_{as}(CH_3)$[a]	2996 (m)[b]	2996 (s)	3015 (vw, sb)[c]	2995 (m, sb)
			3006 (vw, sb)	2992 (m)
			2996 (s)	2990 (m, sb)
$\nu_{s}(CH_3)$	2945 (m)	2945 (m)	2964 (vw, sb)	2941 (m)
			2945 (m)	
ν(CH)	2880 (w)	2880 (w)	2880 (w)	2875 (w)
ν(C=O)	1758 (vs)	1761 (vs)	1777 (vw, sb)	1749 (vs)
			1768 (vw, sb)	
			1759 (vs)	
			1749 (m, sb)	
$\delta_{as}(CH_3)$	1455 (m)	1458 (s)	1468 (w, sb)	1456 (m)
			1458 (s)	1447 (vw, sb)
			1443 (w, sb)	
$\delta_{s}(CH_3)$	1383 (m)	1386 (m)	1396 (vw, sb)	1382 (m)
			1387 (m)	
			1381 (m, sb)	
$\delta_{s}(CH_3)$ + δ(CH)	1365 (m)	1369 (m)	1370 (w)	1368 (m)
		1360 (m)	1360 (m)	
ν_{as}(COC) + $r_{as}(CH_3)$	1213 (m)	1215 (m)	1222 (vw, sb)	1222 (s)
	1183 (s)	1186 (s)	1213 (s)	1216 (s)
			1202 (vw, sb)	1191 (s)
			1184 (m)	
$r_{as}(CH_3)$	1132 (s)	1134 (s)	1144 (vw, sb)	1142 (vw, sb)
			1135 (s)	1132 (s)
ν_{s}(COC)	1092 (s)	1110 (w)	1110 (vw, sb)	1090 (s)
		1092 (s)	1092 (s)	
ν(C−CH_3)	1046 (m)	1046 (m)	1053 (w, sb)	1053 (vw, sb)
			1045 (m)	1042 (s)
$r(CH_3)$ + ν(C−COO)	956 (w)	957 (w)	957 (w)	955 (w)
		924 (w)[d]	924 (w)[d]	908 (w)[d]
			919 (vw, sb)	
ν(C−COO)	870 (m)	872 (m)	872 (m)	874 (w)

[a] ν, δ, and r denote stretching, bending, and rocking, respectively; as and s represent asymmetry and symmetry, respectively. [b] vs, s, m, w, and vw are the abbreviations of very strong, strong, medium, weak, and very weak, respectively. [c] sb denotes the splitting band, whose intensity increases with cooling. [d] Bands at 924 and 908 cm^{-1} are characteristic of the 10_3 helical conformation of homocrystals (α′ and α form) and 3_1 helical conformation of sc crystals, respectively.

existence of weak C−H···O=C hydrogen bonds between the PLLA and PDLA chains in sc crystals.[25,26] Third, the spectral splitting is detected in sc crystals at low temperature, such as the components at 2990 and 2995 cm^{-1} of $\nu_{as}(CH_3)$, 1447 cm^{-1} of $\delta_{as}(CH_3)$, 1153 cm^{-1} of $r(CH_3)$, and 1042 cm^{-1} of ν(C−CH_3) mode. These splitting bands cannot be clearly observed at room temperature and become pronounced with cooling, which is characteristic of the correlation field splitting. Therefore, it is considered that the interchain dipolar interactions related to the carbonyl, methyl, and methine groups exist in the sc crystals (especially at cryogenic conditions), except for the C−H···O=C hydrogen bond interactions. These results imply the tight lateral packing of molecular chains in sc-form PLA.[25,26]

Temperature-Induced Changes in FTIR Intensity and Wavenumber. Temperature-induced changes in the intensity and frequency of various vibrational bands were evaluated based on the FTIR spectra. Intensity changes and frequency shifts of each band were respectively normalized by $[I(T) - I(T_0)]/I(T_0)$ and $WN(T) - WN(T_0)$, where $I(T)$ and $WN(T)$ represented the peak height and wavenumber of a given band at a temperature T, respectively; $I(T_0)$ and $WN(T_0)$ denoted those at an initial temperature T_0, respectively. Here, T_0 was taken as 40 °C for amorphous PLA and 80 °C for the α′-, α-, and sc-form PLAs. Figures 4 and 5 show the normalized intensity changes and frequency shifts of the selected bands for various PLA samples as a function of temperature, respectively. The changes in intensity and wavenumber were found to be reversible upon reheating (data not shown).

As seen in Figures 4 and 5, the intensities gradually increase and most of the bands shift to high wavenumber with cooling, which can be expected since the molecular potential energy drops and the motions of molecular groups become less active with lowering temperature. This phenomenon is analogous to those observed in other polymers,[38,41−43] which has been attributable to the change of interchain forces with temperature.[38] As shown in Figure 4, the temperature-induced intensity changes of amorphous and α′-form PLAs are in the similar ranges (10−20%) with cooling from 40 to −100 °C, which may suggest the weaker interchain interactions in α′ crystals. Obviously, the intensity enhancements of α and sc crystals upon cooling are larger than those of amorphous and α′-form PLAs. Therefore, it is considered that the interchain coupling plays an important role in the temperature-dependent spectral intensity, and the tight packing mode of molecules and more ordered structure increase the sensitivity of spectral intensity to temperature. However, there is not a direct and unambiguous link between the frequency shift and crystal modification for PLA. The values of wavenumber shift in various PLAs are very similar, all of which range 0−4 cm^{-1} with cooling (Figure 5).

Temperature-Dependent Solid-State NMR Spectra. Solid-state structures of different crystals of PLA and amorphous PLA were studied by the solid-state ^{13}C CP-MAS NMR spectroscopy over the temperatures ranging from 80 to −100 °C. Figure 6 shows the temperature-dependent NMR spectra for the carbonyl, methine, and methyl carbons of different crystalline forms of PLA. Each carbon exhibits a single and broad resonance, and no discernible alteration in line shape and chemical shift is detected in the NMR spectra of α′ form with changing temperature (Figure 6 and Figure S4). These findings resemble those observed in amorphous PLA.[51] NMR spectra of α crystals are of much interest (Figure 6 and Figure

dx.doi.org/10.1021/ma201906a | Macromolecules 2012, 45, 189−197

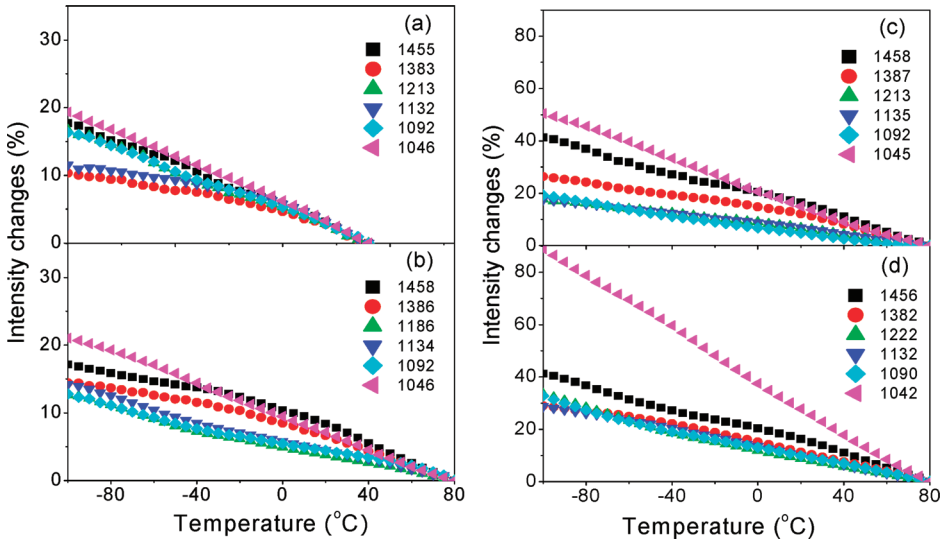

Figure 4. Temperature dependence of normalized intensity changes for FTIR bands of (a) amorphous, (b) α'-, (c) α-, and (d) sc-form PLAs upon cooling.

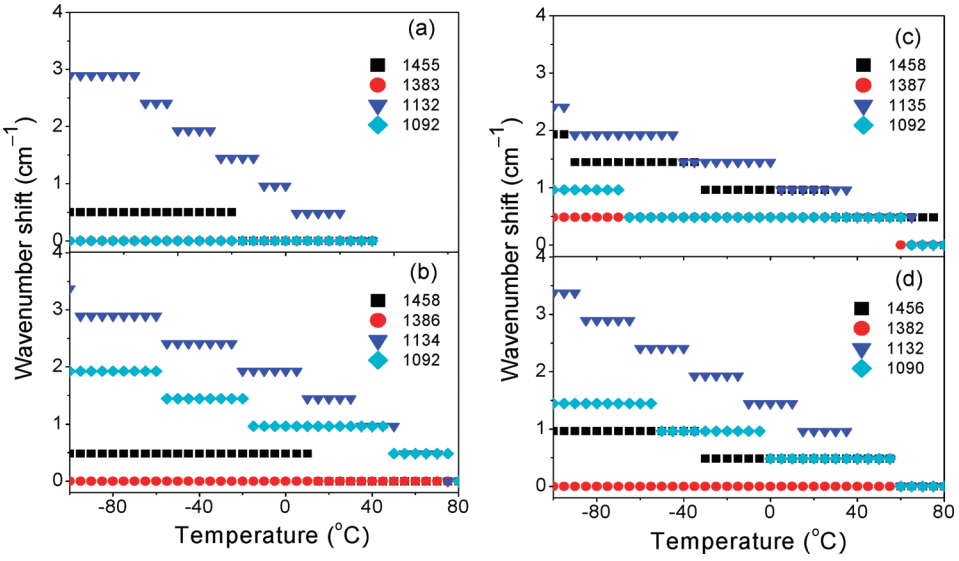

Figure 5. Temperature dependence of wavenumber shifts for FTIR bands of (a) amorphous, (b) α'-, (c) α-, and (d) sc-form PLAs upon cooling.

S5). First, each carbon resonance splits into multiple well-resolved peaks that include four major peaks (P_1–P_4) for carbonyl resonance, three major peaks (P_5–P_7) for methine resonance, and two major peaks (P_8 and P_9) for methyl resonance, where the peaks P_3, P_5, and P_8 are dominant. These results are in agreement with those reported by Thakur et al.[35] and Tsuji et al.[36] Second, chemical shifts of the dominant peaks P_3, P_5, and P_8 are nearly invariable with cooling. However, the splitting peaks gradually shift away from the dominant peaks with lowering temperature. Third, the resonance splitting becomes more marked with cooling, analogous to that observed in the FTIR spectra. The peak shoulders (indicated by arrows in Figure 6 and Figure S5) appear in P_5 and P_8 at low temperature, while they disappear at high temperature.

The difference between NMR spectra of stereoregular PLAs crystallized at low and high temperatures indicates the formation of α' metastable crystals at low T_c (e.g., 80 °C). In the measurements of spin–lattice relaxation, it was found that the splitting peaks for a given carbon of α crystals decayed at a comparable rate, and therefore the splitting peaks could not be assigned individually to amorphous or crystalline component. The resonance splitting can be induced by the intramolecular (e.g., s-PP[31]) or intermolecular (e.g., α-form i-PP[28,29]) interactions in polymer crystals. Because the intrachain interactions that depend on conformation are comparable for α' and α crystals and change little with temperature, the interchain couplings that depend on the lateral molecular packing within crystal lattice may be a predominant contribution to the resonance splittings of α crystals. The splitting peaks in each resonance region represent the crystallographically inequivalent sites in molecular chains. An exact assignment for each split component of α crystals cannot be made from the present results; this needs to be further investigated. It is notable that the resonance splitting in α-form PLA is much more remarkable than that reported in the α-form i-PP[28–30] and i-PB.[33] This is possibly due to the more complicated interchain interactions of α-form PLA, as indicated in the previous studies.[2–6]

dx.doi.org/10.1021/ma201906a | *Macromolecules* 2012, 45, 189–197

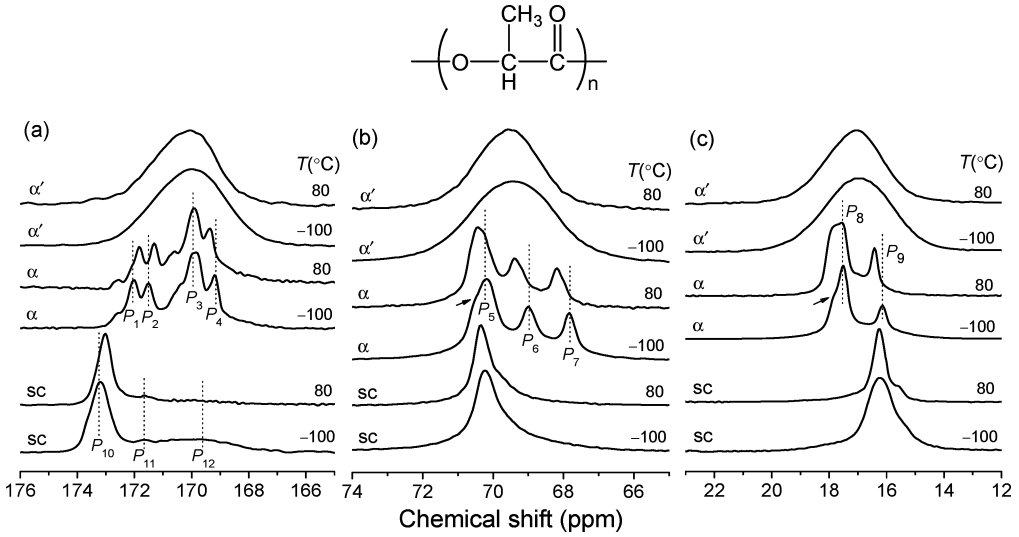

Figure 6. Temperature-dependent ^{13}C CP-MAS NMR spectra for (a) carbonyl, (b) methine, and (c) methyl carbons of different PLA crystals.

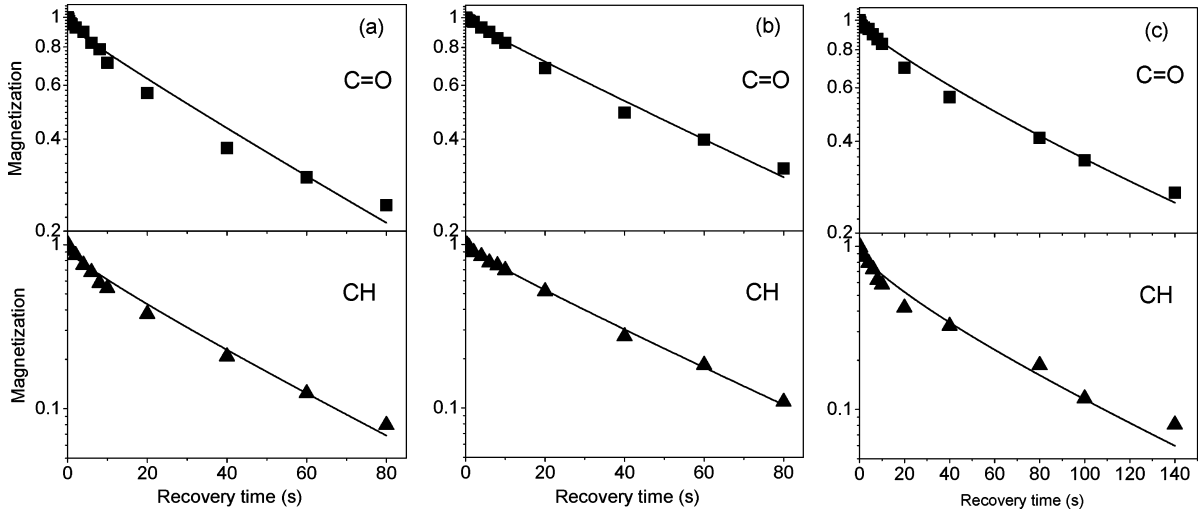

Figure 7. ^{13}C spin−lattice decay curves for carbonyl and methine of (a) α'-, (b) α-, and (c) sc-form PLAs. Solid lines are the fits to the data using eq 1.

The extent of resonance splitting depresses with increasing temperature, similar to those observed in the α crystals of i-PP[30] and i-PB.[33] Upon cooling, the interchain distance decreases accompanied by the strengthening of interchain interactions, accounting for the enhancement in environmental difference between the crystallographically inequivalent sites. At high temperature, more active molecular motion and dipolar exchange between the inequivalent sites can average the line shape and in turn diminish the spectral splitting.[30,33]

The broadening of NMR spectra of α' form is consistent with its FTIR spectra that show broadening compared to the α form. This broadening in NMR spectra resembles the case of β-form i-PP.[28,29] The broadening of ^{13}C CP-MAS NMR spectra can be resulted by many factors such as order/disorder at molecular distances, spherulite shape/size/orientation, etc. However, with combination of the FTIR results that reflect the molecular-level interactions, the NMR spectral broadening and absence of resonance splitting in α' form would suggest its loose and disordered molecular packing. All the carbon atoms in a given group of α' crystals would be in an averaged environment due to the disordered packing mode.

As seen in Figure 6 and Figure S6, sc crystals of PLA exhibit a different ^{13}C solid-state NMR spectrum from the homocrystals, including the line shapes and chemical shifts. As for the sc crystals, three peaks, that is, a sharp peak P_{10}, a weak component P_{11}, and a broad peak P_{12}, are observed in the carbonyl resonance region, while a single sharp peak is basically detected for the methine and methyl resonances. This is consistent with the results reported by Tsuji et al.[37] In the carbonyl resonance region, the peaks P_{10} and P_{11} have been assigned to the crystalline phases of sc and homocrystals, respectively.[37] The broad peak P_{12} is ascribed to the free amorphous phase of PLA, and its chemical shift is very close to the amorphous sample. At temperature above T_g (e.g., 80 °C), the amorphous phase mobility will increase and result in a poor cross-polarization efficiency, leading to the disappearance of P_{12}. Besides, the cold crystallization of free amorphous phase above T_g may also account for the disappearance of P_{12} at 80 °C.

Spin−Lattice Relaxation Time. ^{13}C spin−lattice relaxation measurements were used to assess the molecular dynamics of different crystals of PLA. T_{1C}s of carbonyl and methine

dx.doi.org/10.1021/ma201906a | Macromolecules 2012, 45, 189−197

carbons that had a slower relaxation were only measured. Figure 7 show typical decay curves for the resonances of carbonyl and methine carbons in α′- α-, and sc-form PLAs measured at ∼25 °C. The decay curve of amorphous PLA is shown elsewhere.[51] Because the molecular motions in both amorphous and crystalline phases must be highly restricted below T_g, the relaxation time of amorphous and crystalline phases of semicrystalline PLA will be in a similar order of magnitude (or comparable) at a temperature below T_g (∼60 °C for PLA). As reported in a previous study,[51] the decay curve of spin−lattice relaxation of the fully amorphous PLA can be well fitted by the Kohlraush−Williams−Watts (KWW) function,[52,53] which is generally used to express the magnetization below T_g because the distribution of relaxation rate usually gives rise to a nonexponential recovery.[52] To evaluate the T_{1C} of semicrystalline PLAs, we add an exponential term to the KWW function to reflect the contribution of crystalline phase. The equation used for fitting is expressed as

$$M_z(t) \propto (1 - X_c)\exp\left[\left(\frac{-t}{T_{1C,a}}\right)^{\beta}\right] + X_c \exp\left(\frac{-t}{T_{1C,c}}\right) \quad (1)$$

where the first (KWW function) and second terms denote the contributions of amorphous and crystalline phases, respectively. M_z is the normalized magnetization, and t is the relaxation time that is a variable used in the experiment. X_c is the degree of crystallinity, as shown in Table 1. $T_{1C,c}$ is the T_{1C} of crystalline phase. $T_{1C,a}$ is the T_{1C} of amorphous phase in the semicrystalline or fully amorphous PLA. β is a stretching parameter ($0 < \beta \leq 1$) of the KWW function, representing the deviation of relaxation from the pure exponential nature.[52,53] $T_{1C,a}$ and β are 54.1 s and 0.898 for the carbonyl carbon and 22.8 s and 0.859 for the methine carbon of amorphous PLA, respectively, as determined in our previous report.[51]

T_{1C} of the crystalline phase ($T_{1C,c}$) of α′-, α-, and sc-form PLAs were estimated by fitting the normalized magnetization in spin−lattice relaxation using eq 1. The results of T_{1C} are tabulated in Table 3. The mean T_{1C} of amorphous PLA, $\langle T_{1C,a}\rangle$, is included for comparison. As seen in Table 3, T_{1C} of PLA depends on the crystalline structure remarkably. The relaxation time, usually inversely proportional to relaxation rate and molecular mobility, increases in the order of amorphous ≈ α′ < α < sc for PLA below T_g. For protonated carbons, the fluctuation of C−H dipolar coupling is the predominant relaxation. This can include three contributions, that is, coupling of carbon atom with (i) directly bonded protons, (ii) intrachain, or (iii) interchain nonbonded nearby protons.[27] The strength of dipolar interaction depends on internuclear distance between ^{13}C and ^{1}H. It ranks in the order of (i) directly bonded protons > (ii) intrachain > (iii) interchain nonbonded nearby protons, and the resultant relaxation time should be T_{1C} (i) < T_{1C} (ii) < T_{1C} (iii). On the other hand, tight packing probably inhibits local mobility, resulting in a longer T_{1C}. The carbonyl carbons have slower relaxation rate compared to protonated carbons because of the weak C−H dipolar interaction. The contribution (i) may be the same for different PLA samples because of the identical bond lengths. The contribution (ii), depending on the conformation, is considered to be similar for the α′ and α crystals, while might be larger for sc crystals because of the more contracted conformation. The contribution (iii), which has been reported to be a crucial factor influencing the relaxation time of various polymorphs of poly(3-hydroxypropionate) (PHP),[42] depends on the lateral interchain distance. It is considered that the lateral molecular packing is a key factor for the different molecular dynamics of various PLA crystals. The very similar relaxation rate of the α′ crystals and amorphous PLA further confirms the disordered and looser molecular packing of α′ crystals, which is somewhat analogous to the amorphous sample. Because of the tighter packing and shorter interchain distance, α crystals exhibit a slower relaxation than their α′ counterparts. In the case of sc crystals, two racemic chains with opposite handedness allow the tighter packing and smaller interchain distance within crystal cell, which may account for the slower relaxation.

Table 3. Spin−Lattice Relaxation Times of Amorphous, α′-, α-, and sc-Form PLAs

parameters	carbon	amorphous	α′	α	sc
$\langle T_{1C,a}\rangle^a$ (s)	C=O	57.0			
	CH	24.7			
$T_{1C,c}$ (s)	C=O		52.1	73.5	151.5
	CH		29.4	40.0	66.2

[a]The mean T_{1c} value of amorphous PLA was cited from ref 51.

CONCLUSION

The molecular interaction, packing, and dynamics in various crystal forms of PLA have been investigated by the temperature-variable FTIR and solid-state ^{13}C NMR spectroscopy. The different crystal forms of PLA show distinct spectral features in line shapes and band/resonance splittings upon cooling to the cryogenic conditions. The well-resolved splittings in FTIR bands and NMR resonances of α-form PLA are ascribed to the correlation field splitting and crystallographically inequivalent sites within the crystal lattices, respectively; however, these splitting are absent in PLA α′ crystals. These results indicate the conformational disorder and loose molecular packing in the α′ crystals of stereoregular PLA crystallized at low temperature. As a result of the tight lateral molecular packing, the interchain interactions exist extensively between the two antiparallel packed chains within the lattice of α-form PLA; it is predominantly the dipolar interactions involving carbonyl, methyl, and methine groups. The frequency shifts in stereocomplex crystallization and the correlation field splittings at cryogenic conditions suggest the coexistence of weak C−H···O=C hydrogen bonds and dipolar interactions between the PLLA and PDLA chains packed in sc crystals of PLA. The spin−lattice relaxation times of various PLA crystals rank as amorphous ≈ α′ < α < sc below T_g. In a word, the lateral arrangement and packing of molecular chains in the crystalline phase, which are the origin of the interchain interactions, play an important role in the polymorphism of PLA. This would be an important factor influencing the physical proprieties (e.g., mechanical, barrier properties, and biodegradability) of PLA materials.

ASSOCIATED CONTENT

Supporting Information

Figures showing temperature-dependent FTIR spectra and ^{13}C CP-MAS NMR spectra of PLLA with different crystalline

forms. This material is available free of charge via the Internet at http://pubs.acs.org.

AUTHOR INFORMATION

Corresponding Author

*Tel +86-571-87951334; e-mail panpengju@zju.edu.cn.

ACKNOWLEDGMENTS

We are grateful to Dr. Kazue Ueda (Unitika Co. Ltd.) for kindly supplying PLLA samples, Prof. Minoru Sakurai (Tokyo Institute of Technology) for the use of FTIR instrument, and Dr. Tadashi Shimizu and Dr. Masataka Tansho (National Institute of Material Science) for the use of solid-state NMR instrument. Financial support from State Key Laboratory of Chemical Engineering (SKL-ChE-11D05), Fundamental Research Funds for the Central Universities, and National Natural Science Foundation of China (51103127) is greatly appreciated.

REFERENCES

(1) Auras, R.; Lim, L.-T.; Selke, S. E. M.; Tsuji, H. *Poly(lactic acid): Synthesis, Structures, Properties, Processing, and Applications*; John Wiley & Son: Hoboken, NJ, 2010.
(2) De Santis, P.; Kovacs, A. J. *Biopolymers* **1968**, *6*, 299.
(3) Hoogsteen, W.; Postema, A. R.; Pennings, A. J.; ten Brinke, G.; Zugenmaier, P. *Macromolecules* **1990**, *23*, 634.
(4) Kobayashi, J.; Asahi, T.; Ichiki, M.; Oikawa, A.; Suzuki, H.; Watanabe, T.; Fukada, E.; Shikinami, Y. *J. Appl. Phys.* **1995**, *77*, 2957.
(5) Aleman, C.; Lotz, B.; Puiggali, J. *Macromolecules* **2001**, *34*, 4795.
(6) Sasaki, S.; Asakura, T. *Macromolecules* **2003**, *36*, 8385.
(7) Eling, B.; Gogolewski, S.; Pennings, A. J. *Polymer* **1982**, *23*, 1587.
(8) Sawai, D.; Takahashi, K.; Sasashige, A.; Kanamoto, T.; Hyon, S. H. *Macromolecules* **2003**, *36*, 3601.
(9) Cartier, L.; Okihara, T.; Ikada, Y.; Tsuji, H.; Puiggali, J.; Lotz, B. *Polymer* **2000**, *41*, 8909.
(10) Zhang, J.; Duan, Y.; Sato, H.; Tsuji, H.; Noda, I.; Yan, S.; Ozaki, Y. *Macromolecules* **2005**, *38*, 8012.
(11) Zhang, J.; Tashiro, K.; Domb, A. J.; Tsuji, H. *Macromol. Symp.* **2006**, *242*, 274.
(12) Pan, P.; Kai, W.; Zhu, B.; Dong, T.; Inoue, Y. *Macromolecules* **2007**, *40*, 6898.
(13) Kawai, T.; Rahman, N.; Matsuba, G.; Nishida, K.; Kanaya, T.; Nakano, M.; Okamoto, H.; Kawada, J.; Usuki, A.; Honma, N.; Nakajima, K.; Matsuda, M. *Macromolecules* **2007**, *40*, 9463.
(14) Zhang, J.; Tashiro, K.; Domb, A. J.; Tsuji, H. *Macromolecules* **2008**, *41*, 1352.
(15) Yasuniwa, M.; Sakamo, K.; Ono, Y.; Kawahara, W. *Polymer* **2008**, *49*, 1943.
(16) Pan, P.; Inoue, Y. *Prog. Polym. Sci.* **2009**, *34*, 605.
(17) Furuhashi, Y.; Iwata, T.; Kimura, Y.; Doi, Y. *Macromol. Biosci.* **2003**, *3*, 462.
(18) Gan, Z.; Kuwabara, K.; Abe, H.; Iwata, T.; Doi, Y. *Polym. Degrad. Stab.* **2005**, *87*, 191.
(19) Sawai, D.; Yokoyama, T.; Kanamoto, T.; Sungil, M.; Hyon, S. H.; Myasnikova, L. P. *Macromol. Symp.* **2006**, *242*, 93.
(20) Cocca, M.; Di Lorenzo, M. L.; Malinconico, M.; Frezza, V. *Eur. Polym. J.* **2011**, *47*, 1073.
(21) Kalish, J. P.; Aou, K.; Yang, X. Z.; Hsu, S. L. *Polymer* **2011**, *52*, 814.
(22) Okihara, T.; Tsuji, M.; Kawaguchi, A.; Katayama, K.-I.; Tsuji, H.; Hyon, S.-H.; Ikada, Y. *J. Macromol. Sci., Phys.* **1991**, *B30*, 119.
(23) Tsuji, H. *Macromol. Biosci.* **2005**, *5*, 569.
(24) Brizzolara, D.; Cantow, H. J.; Diederichs, K.; Keller, E.; Domb, A. J. *Macromolecules* **1996**, *29*, 191.
(25) Zhang, J.; Sato, H.; Tsuji, H.; Noda, I.; Ozaki, Y. *Macromolecules* **2005**, *38*, 1822.
(26) Sarasua, J. R.; Rodríguez, N. L.; Arraiza, A. L.; Meaurio, E. *Macromolecules* **2005**, *38*, 8362.
(27) Mirau, P. A. *A Practical Guide to Understanding the NMR of Polymers*; Wiley-Interscience: Hoboken, NJ, 2005.
(28) Bunn, A.; Cudby, M. E. A.; Harris, R. K.; Packer, K. J.; Say, B. J. *Polymer* **1982**, *23*, 694.
(29) Gomez, M. A.; Tanaka, H.; Tonelli, A. E. *Polymer* **1987**, *28*, 2227.
(30) Saito, S.; Moteki, Y.; Nakagawa, M.; Horii, F.; Kitamaru, R. *Macromolecules* **1990**, *23*, 3256.
(31) Bunn, A.; Cudby, M. E. A.; Harris, R. K.; Packer, K. J.; Say, B. J. *J. Chem. Soc., Chem. Commun.* **1981**, 15.
(32) Ohira, Y.; Horii, F.; Nakaoki, T. *Macromolecules* **2001**, *34*, 1655.
(33) Miyoshi, T.; Hayashi, S.; Imashiro, F.; Kaito, A. *Macromolecules* **2002**, *35*, 2624.
(34) Howe, C.; Vasanthan, N.; MacClamrock, C.; Sankar, S.; Shin, I. D.; Simonsen, I. K.; Tonelli, A. E. *Macromolecules* **1994**, *27*, 7433.
(35) Thakur, K.; A., M.; Kean, R. T.; Zupfer, J. M.; Buehler, N. U.; Doscotch, M. A.; Munson, E. J. *Macromolecules* **1996**, *29*, 8844.
(36) Tsuji, H.; Kamo, S.; Horii, F. *Polymer* **2010**, *51*, 2215.
(37) Tsuji, H.; Horii, F.; Nakagawa, M.; Ikada, Y.; Odani, H.; Kitamaru, R. *Macromolecules* **1992**, *25*, 4114.
(38) Takahashi, Y. *Macromolecules* **2001**, *34*, 7836.
(39) Davis, G. T.; Eby, R. K.; Colson, J. P. *J. Appl. Phys.* **1970**, *41*, 4316.
(40) Lacks, D. J.; Rutledge, G. C. *Macromolecules* **1995**, *28*, 1115.
(41) Snyder, R. G.; Maroncelli, M.; Strauss, H. L.; Hallmark, V. M. *J. Phys. Chem.* **1986**, *90*, 5623.
(42) Su, Z.; Zhao, Y.; Kang, N.; Zhang, X.; Xu, Y.; Wu, J.; Wang, D.; Han, C. C.; Xu, D. *Macromol. Rapid Commun.* **2005**, *26*, 895.
(43) Zhu, B.; Kai, W.; Pan, P.; Yazawa, K.; Nishida, H.; Sakurai, M.; Inoue, Y. *J. Phys. Chem. B* **2008**, *112*, 9684.
(44) Torchia, D. A. *J. Magn. Reson.* **1978**, *30*, 613.
(45) Fischer, E. W.; Sterzel, H. J.; Wegner, G. *Kolloid Z. Z. Polym.* **1973**, *251*, 980.
(46) Loomis, G. L.; Murdoch, J. R.; Gardner, K. H. *Polym. Prepr.* **1990**, *31*, 55.
(47) Kister, G.; Cassanas, G.; Vert, M. *Polymer* **1998**, *39*, 267.
(48) Meaurio, E.; Zuza, E.; Lopez-Rodriguez, N.; Sarasua, J. R. *J. Phys. Chem. B* **2006**, *110*, 5790.
(49) Aou, K.; Hsu, S. L. *Macromolecules* **2006**, *39*, 3337.
(50) Lagaron, J. M.; Powell, A. K.; Davidson, N. S. *Macromolecules* **2000**, *33*, 1030.
(51) Pan, P.; Zhu, B.; Dong, T.; Yazawa, K.; Shimizu, T.; Tansho, M.; Inoue, Y. *J. Chem. Phys.* **2008**, *129*, 184902.
(52) Böhmer, R.; Diezemann, G.; Hinze, G.; Rössler, E. *Prog. Nucl. Magn. Reson. Spectrosc.* **2001**, *39*, 191.
(53) Yazawa, K.; Inoue, Y.; Yamamoto, T.; Asakawa, N. *Phys. Rev. B* **2006**, *74*, 094204.